Available online at www.sciencedirect.com
SCIENCE DIRECT
Journal of volcanology and geothermal research
ELSEVIER
Journal of Volcanology and Geothermal Research 152 (2006) 121–139
www.elsevier.com/locate/jvolgeores

Shallow velocity structure and seismic site effects at Arenal volcano, Costa Rica

Mauricio M. Mora [a,b,*], Philippe Lesage [a,c], Bernard Valette [a,c], Guillermo E. Alvarado [b,d], Carlos Leandro [d], Jean-Philippe Métaxian [a,c], Jacques Dorel [e]

[a] *Laboratoire de Géophysique Interne et Tectonophysique, Université de Savoie, 73376 Le Bourget-du-Lac, France*
[b] *Escuela Centroamericana de Geología, Universidad de Costa Rica, San José, Costa Rica*
[c] *Institut de Recherche pour le Développement, France*
[d] *Observatorio Sismológico y Vulcanológico de Arenal y Miravalles, Instituto Costarricense de Electricidad, Costa Rica*
[e] *Observatoire de Physique du Globe, Clermont-Ferrand, France*

Received 28 December 2004; received in revised form 9 July 2005; accepted 23 September 2005
Available online 15 December 2005

Abstract

We use the spatial autocorrelation (SPAC) method with improved inversion algorithms to estimate the Love and Rayleigh dispersion curves at two sites at the West and Northeast flanks of Arenal volcano, Costa Rica. At the West flank site, the Rayleigh waves phase velocities vary from 765 m s^{-1} at 1 Hz to 300 m s^{-1} at 12 Hz and those of Love waves between 780 and 295 m s^{-1} in the same frequency band. At the Northeast flank site, the Rayleigh wave velocities range from 1386 to 300 m s^{-1} and those of Love from 1983 to 315 m s^{-1}. From dispersion curves we derive shallow (<400 m) P and S waves velocity models. 2D velocity models down to a depth of 150 m are also obtained by seismic refraction surveys along two radial profiles on the tephra apron at West and East flanks. They present strong vertical and lateral variations in the velocity and thickness of the layers.

Strong variations in amplitude of the spectral peaks are observed for the seismic events along two radial arrays. These site effects are analysed using the H/V spectral ratio method and S-wave theoretical transfer functions. Results show that the wave amplifications are related to resonance effects of shallow structure (<150 m) and occur only where impedance contrast with the deeper layers is strong enough. In contrast, almost no site effect are detected at the Masaya shield volcano, Nicaragua, where the structure is more homogeneous and mainly composed of lava flows.

When a resonance of the shallow layers occurs, the correlation coefficients between close stations increase at the corresponding frequency. The site effects may thus produce spurious results with the SPAC method. The H/V spectral ratio, used in complement of the SPAC method, can help detecting the site effects and testing the plane layer hypothesis. Furthermore, the theoretical transfer functions calculated for the estimated velocity models is also useful to validate the models.

Keywords: volcanic seismology; seismic site effect; velocity structure; SPAC method; H/V spectral ratio; Arenal volcano; Masaya volcano

1. Introduction

Arenal volcano is a small (1100 m high, 1670 m above sea level, 15 km^3) basaltic andesite stratovolcano located in northwestern Costa Rica (Fig. 1). It began to form 7000 B.P. by superposition of lava fields, pyro-

* Corresponding author. Escuela Centroamericana de Geología, Universidad de Costa Rica, San José, Costa Rica. Tel.: +506 253 8407; fax: +506 253 2586.
E-mail address: mmmora@geologia.ucr.ac.cr (M.M. Mora).

0377-0273/$ - see front matter © 2005 Elsevier B.V. All rights reserved.
doi:10.1016/j.jvolgeores.2005.09.013

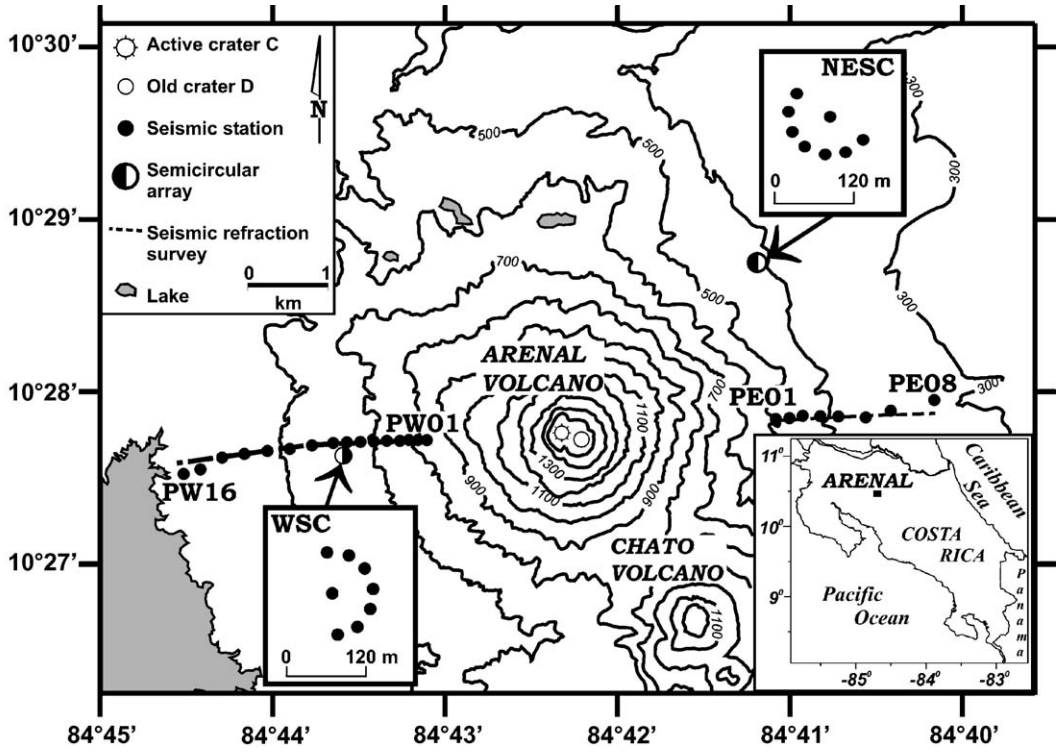

Fig. 1. Map of Arenal volcano indicating the location and configuration of the linear and semicircular arrays and the seismic refraction surveys used in this study. WSC: west semicircular array. NESC: northeast semicircular array. PW: west radial array. PE: east radial array.

clastic and epiclastic deposits. Rocks from the volcano basement are older than 20 000 years and include tephra, tuffs, lahars and lava flows, all of them mildly to deeply weathered (Soto et al., 1998; Alvarado et al., 2003). Arenal began a lateral explosive eruption in July 29, 1968, resulting in 78 deaths and 230 km^2 of damage including villages and cattle fields (Melson and Sáenz, 1968). This eruption started with a closed-conduit pelean eruption that formed 3 new craters at the West flank. Those craters together with the previous crater D are evidence of an East–West fracture system. Arenal present activity is located at crater C, from which a hundred of thin and small blocky lava flows had been erupted up to now, forming a lava field that covers 7.5 km^2 and has a volume of 0.75 km^3 (Borgia et al., 1988; Alvarado and Soto, 2002). Arenal activity is also characterized by Strombolian eruptions, lava avalanches, and sporadic pyroclastic flows.

The generation of a large variety of seismic signals, such as harmonic and spasmodic tremor, explosion quakes and long-period (LP) events, is characteristic of the present volcanic activity at Arenal. Harmonic tremor has a fundamental frequency lying in the range [0.9–2] Hz with up to ten overtones (Hagerty et al., 2000; Mora, 2003), whereas spasmodic tremor, explosions and LP events present a frequency band ranging from 1 to 10 Hz. Explosion quakes are sometimes accompanied by an audible air-shock wave arriving several seconds after the P-wave onset and their coda frequently become harmonic tremor (e.g. Alvarado and Barquero, 1987; Benoit and McNutt, 1997). The corresponding seismic sources are localized beneath the active crater (Hagerty et al., 2000; Métaxian et al., 2002).

Like Arenal, most volcanoes are complex and heterogeneous structures characterized by alternations of strata with very different mechanical properties, such as lava flows and pyroclastic deposits that produce strong perturbations of the seismic wavefield. For example, free surface and shallow stratigraphic effects can modify the wave polarization, especially at low frequency (Neuberg and Pointer, 2000; Hellweg, 2003). Strong lateral heterogeneities or uneven topography can induce wave scattering (La Rocca et al., 2001) or ray deflection from the vertical plane (e.g. Weiland et al., 1995). In some cases, scattering generates rapid attenuation of the direct waves and lost of coherence at short distances (Wegler and Lühr, 2001). Local amplifications of the seismic waves have been observed at Stromboli, Italy (Del Pezzo et al., 1974; Ntepe and Dorel, 1990; Falsaperla et al., 1992), Klyuchevskoy, Kamchatka (Gordeev et al., 1989, 1990) and Sakurajima, Japan (Tsuruga et

al., 1997). These amplifications generally occur in narrow spectral bands, producing spectral peaks that may be mixed up with source effects (Gordeev et al., 1990; Gordeev, 1993; Goldstein and Chouet, 1994; Kedar et al., 1998; Mora et al., 2001). In order to avoid misinterpretations due to perturbations of the wavefield, it is necessary to identify both local site effects and the influence of the shallow structure on the seismic waves.

In this paper we present a study of the shallow structure and associated site effects at Arenal volcano, which is based on the combination of several approaches. Velocity structures are obtained by two seismic refraction profiles, and two surveys carried out by using the spatial autocorrelation method (Aki, 1957). Local amplifications of the seismic waves are detected by applying the H/V spectral ratios method (Nakamura, 1989). Theoretical S-wave transfer functions are then calculated from the velocity models and are compared to the spectral ratios. This makes it possible to verify the relationship between the shallow structure and the observed site effects, and to check the consistency of the velocity model. A comparative study of the H/V spectral ratios with Masaya shield volcano, Nicaragua, is also carried out in this work. The large differences observed in the site effects detected at both volcanoes confirm the strong influence of the shallow structure on the wavefield.

2. Instrumentation and data

The data analysed in this paper were recorded in 1997 by two radial and two semicircular arrays (Fig. 1). The East radial array was 1.9 km long and included 8 stations located 150–500 m apart, with the first station at about 2.5 km from the active crater. The West radial array was 2.9 km long and consisted of 16 stations located 100–260 m apart, with the first station at approximately 1.5 km from the crater. The semicircular arrays were deployed 3 km NE and 2.6 km W from the crater. Both had a radius of 60 m and were composed of 8 receivers located every 30°. All the arrays were equipped with three-component Mark Products L-22 seismometers with natural frequency of 2 Hz and flat response up to 25 Hz. All sensors were buried in 40 cm deep holes to reduce environmental noise. Recording was performed in continuous mode using SISMALP3 digital acquisition systems with a sampling rate of 100 Hz. Synchronization was obtained using external LOCSAT GPS systems. These arrays were part of a largest seismic experiment carried out by French and Costa Rican institutions, in which several small aperture arrays of different configurations were deployed around Arenal volcano in January and February 1997, to study the source and wavefield of tremor and LP events.

In a second stage of the experiment, the Instituto Costarricense de Electricidad (ICE) carried out two seismic refraction profiles along the radial arrays with a 48-channel 20 bits StrataVizor NZ Geometrics recorder and 12 Hz natural frequency geophones. The receivers were located 10 m apart, and the source offset was 100 m. Explosives were buried at a depth of 1.5–2 m. The errors on the topographic profile and position of the receivers are, respectively, ± 50 cm and ± 40 cm. The errors on the arrival times lectures are ± 2 ms. Parallel to the seismic refraction profiles, ICE also carried out vertical Schlumberger geoelectric surveys every 200 m, with a maximum aperture of 1000 m, to better constrain the depths of interfaces and water table (Leandro and Alvarado, 1999).

3. 2D velocity models obtained by seismic refraction surveys

The seismic refraction data were analysed using the reciprocal method, also known as the Hagiwara's method (Hagiwara and Omote, 1939). The error on the estimation of the depth of the interfaces is cumulative and can reach 15%. This means that for each layer (except for the first one) the determination of the interfaces depends on the estimation of the previous one. The interpretation of the seismic structure in terms of material is based on geological observations around the volcano (Borgia et al., 1988; Leandro and Alvarado, 1999; Alvarado et al., 2003). The detailed seismic refraction surveys provide 2-D shallow (down to a 150-m depth) P-wave velocity models (Fig. 2). Although the main features of the models appears robust, difficulties arising from phase reading and interpretation or from complexities of the seismic sections may yield lack of accuracy in some details of the obtained structure. This is composed by three main layers. At the top, a $V_p < 1.95$ km s^{-1} layer can be associated to poorly consolidated tephras. This unit is thicker on the west flank (25–140 m) than at the east one (20–50 m). The next layer is characterized by V_p ranging from 2.1 to 3.6 km s^{-1}. It might correspond to breccia and lava flows at the west and east flanks, respectively. The last layer could be the local basement probably associated to pre-Arenal volcanic rocks (Leandro and Alvarado, 1999).

More precisely, the refraction surveys reveal that the tephra unit is subdivided into minor layers of different types of pyroclastic and epiclastic deposits. On the west flank, close to the PW01 site, the tephra unit can be correlated to a 22-m-thick sequence,

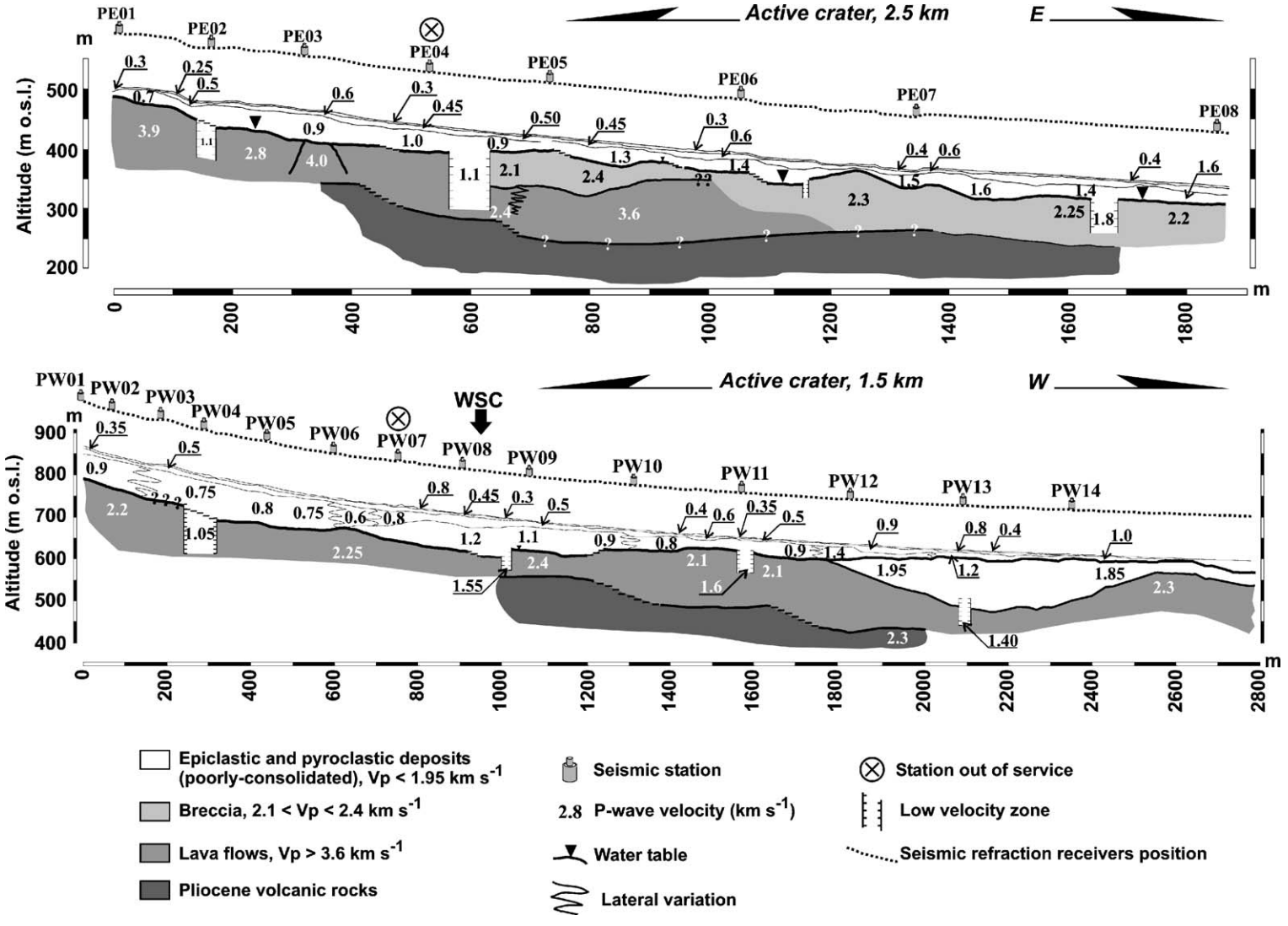

Fig. 2. Shallow P-wave velocity structures interpreted from the seismic refraction surveys for the east (top) and west (bottom) flanks of Arenal volcano. The water table was obtained from geoelectric measurements along the seismic profile (Leandro and Alvarado, 1999).

formed by phreatomagmatic basaltic explosions (~1000 A.D.), overlaid by reworked deposits and by the 1968 eruption tephras (Soto et al., 2000). On both flanks, the whole structure presents strong lateral variations in velocities and resistivities, as well as in layer thickness, which reflects rapid changes in material properties, such as the degree of consolidation, the grain size and the degree of alteration.

The seismic refraction surveys also show several P-wave low-velocity anomalies, which can be closely related to Holocene active faults, oriented mainly N–S, NW–SE and WNW–ESE that are cutting the present Arenal edifice (Leandro and Alvarado, 1999; Alvarado et al., 2003).The anomaly with V_p=1.1 km s^{-1} situated at a distance of 600 m from the upper end of the east profile is related to a NW–SE fault located along the northern flank of Arenal and to which hot springs are associated (Soto et al., 1999). The 1.8 km s^{-1} anomaly at 1650 m is an evidence for the Aguacaliente fault, which has a SW–NE orientation and is located between Arenal and Chato volcanoes. Less is known from the geological point of view about the structure of the western flank, because of the recent lava and tephra deposits that cover this side. Four P-wave low-velocity anomalies are detected along the west profile. From these, only the anomaly at 300 m (V_p=1.05 km s^{-1}) may be related to a NE–SW fault.

4. Velocity models from array analysis of surface waves

The spatial autocorrelation method, also known as the SPAC method, was first designed by Aki (1957) to analyse the background seismic noise and has become a common tool for studying the shallow seismic structure in volcanic contexts. The basic assumption of the method is that the wave field is stochastic and stationary in time and space. A relationship between the spectra of the waves in time and space is used to provide information on the properties of the wavefield. A detailed explanation of the method can be found in Ferrazzini et al. (1991), Chouet (1996) and Métaxian et al. (1997). The method was applied by Wada and Ono (1965) to study the volcanic tremor at Aso (Japan) and later by Ferrazzini et al. (1991) to analyse the volcanic wavefield at Kilauea (Hawaii). The latter authors showed that the wavefield generated by tremors and gas-piston events is composed of 60% of Rayleigh waves and 40% of Love waves at 0.9 km from the Puu-Oo crater. They also determined phase velocities varying from 700 m s^{-1} at 2 Hz to 300 m s^{-1} at 8 Hz. Métaxian et al. (1997) applied the SPAC method at Masaya volcano (Nicaragua). They observed that tremor contains equal proportions of Rayleigh and Love waves. Love phase velocities range from 730 to 1240 m s^{-1} at 2 Hz and from 330 to 550 m s^{-1} at 6 Hz depending on the site. Rayleigh waves velocities range from 930–1100 m s^{-1} at 2 Hz to 330–440 m s^{-1} at 6 Hz. The spatial correlation technique was also applied at Stromboli, Italy (Chouet et al., 1998a,b), Deception Island, Antartic (Saccorotti et al., 2001a) and Kilauea, Hawaii (Saccorotti et al., 2003). Saccorotti et al. (2001b) used a non-circular array of 20 seismometers at Vesuvius, Italy and Bettig et al. (2003) proposed a more rigorous procedure to generalize Aki's method to irregular arrays.

We applied the SPAC method to determine velocity models at two sites on the west and northeast flanks of Arenal volcano. For each semicircular array we selected 30 min of non-continuous records of stationary spasmodic tremor (Fig. 3). For each component (vertical, radial or transverse) the records were divided in 81.92 s-long slices and were filtered in the frequency domain using a 0.25 Hz boxcar window. For each slice and each frequency band, centered on frequency ω and stepped in increments of 0.1 Hz, we calculated the normalized correlation coefficients $\rho_n(r,\varphi,\omega)$ between the receiver located at the hub of the array and those located at the circumference, with polar coordinates (r,φ) where r is the semicircle radius and φ the azimuth of the line connecting the two sensors. We showed that the correlation coefficients are almost independent of the type of signal used and that similar results can be obtained with harmonic tremor (Mora, 2003).

However, as pointed out by Vandecar and Crosson (1990) and Saccorotti and Del Pezzo (2000), the statistical distribution of the coefficients $\rho_n(r,\varphi,\omega)$ cannot be Gaussian since they are bounded. Hence the arithmetic average of the correlation coefficients can be biased. Following Saccorotti and Del Pezzo (2000), we calculated the Fisher's transform of the normalized correlation coefficients:

$$z_n(r,\varphi,\omega)=\frac{1}{2}\ln\left[\frac{1+\rho_n(r,\varphi,\omega)}{1-\rho_n(r,\varphi,\omega)}\right]. \quad (1)$$

The inverse transform ρ_a of the arithmetic average of functions z_n

$$\rho_a(r,\varphi,\omega)=\tanh(z_a(r,\varphi,\omega)) \quad (2)$$

with:

$$z_a(r,\varphi,\omega)=\frac{1}{N}\sum_{n=1}^{N} z_n(r,\varphi,\omega) \quad (3)$$

ranges between -1 and $+1$ and is an unbiased estimate of the averaged coefficient. Actually, coefficients ρ_a are

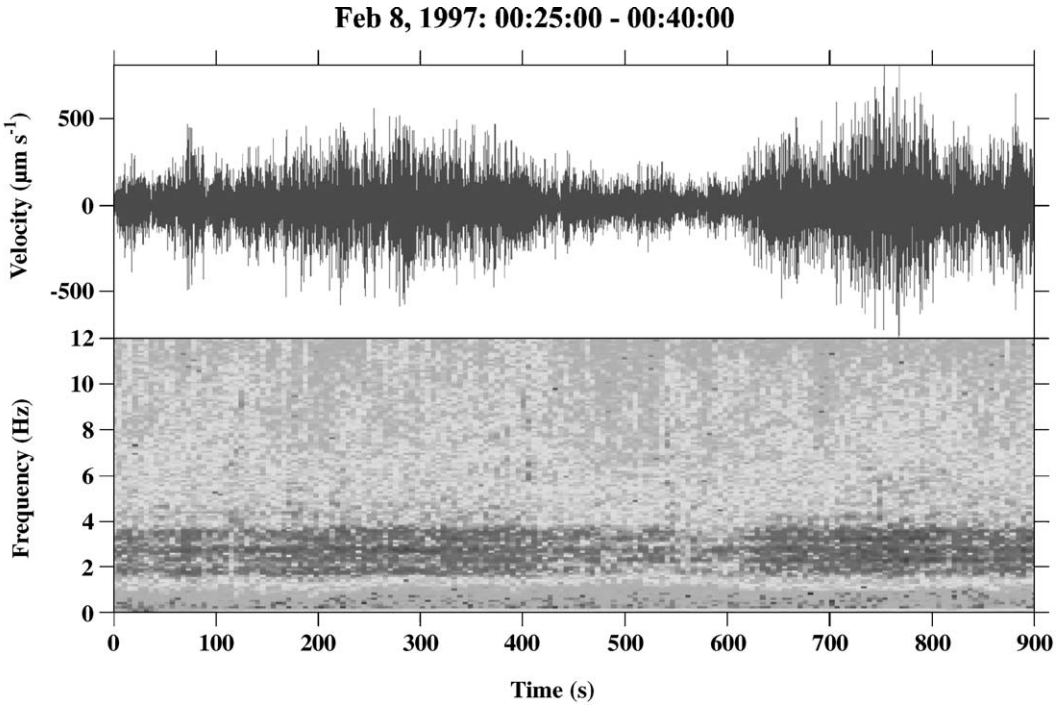

Fig. 3. Seismogram (top) and spectrogram (bottom) of a spasmodic tremor slice recorded on a vertical component of the NE semicircular array. Date and time interval of the record are shown at the top of the figure. The signal is quite stationary and most of its energy is concentrated in the [1–4] Hz band. The spectrogram was calculated using a 10.24 s long moving window with 5.12 s shift.

very close to the arithmetic averages of ρ_n. Correct to first order, its standard deviation σ_{ρ_a} can be obtained from the standard deviation of z_a through:

$$\sigma_{\rho_a} = \left|\frac{\mathrm{dtanh}(z_a)}{\mathrm{d}z_a}\right|\sigma_{z_a} = |1-\tanh^2(z_a)|\sigma_{z_a}. \quad (4)$$

For a fixed radius r, the average correlation coefficients are displayed in Fig. 4. No predominant propagation direction is observed at the NE array. On the W array, slightly elongated ellipsoids with major axes oriented NS are observed in the [1–4] Hz range, indicating wave propagation in the EW azimuth, which is consistent with the source position.

The azimuthal average of the correlation coefficients, and the corresponding variances, can be calculated as:

$$\sigma_{\rho_a} = \left|\frac{\mathrm{dtanh}(z_a)}{\mathrm{d}z_a}\right|\sigma_{z_a} = |1-\tanh^2(z_a)|\sigma_{z_a},\ \bar{\rho}(r,\omega)$$

$$= \frac{1}{\pi}\int_0^{\pi} \rho_a(r,\phi,\omega)\mathrm{d}\phi \quad (5)$$

$$\bar{\sigma}^2(r,\omega) = \frac{1}{\pi}\int_0^{\pi} \sigma^2(r,\varphi,\omega)\mathrm{d}\varphi. \quad (6)$$

However, this expression of the variance only reflects the fluctuations between the signal slices and it does not account for other errors, such as systematic bias. To take account of this, we added a constant term equal to the mean value of the variance over the frequency interval considered $[\omega_1, \omega_2]$, which yields:

$$\bar{\sigma}_f^2(r,\omega) = \bar{\sigma}^2(r,\omega) + \frac{1}{\omega_2-\omega_1}\int_{\omega_1}^{\omega_2} \bar{\sigma}^2(r,\omega')\mathrm{d}\omega'. \quad (7)$$

The azimuthal average coefficients with their errors are shown in Fig. 5. We can note a marked increase of the coefficients in the range [4–6] Hz for the NE array. We will come back to this point later.

Aki (1957) showed that the azimuthally averaged correlation coefficients can be related to the phase velocities through Bessel functions as:

$$\begin{aligned}\bar{\rho}_v(r,\omega) &= J_0(x_R)\\ \bar{\rho}_r(r,\omega) &= \alpha[J_0(x_R)-J_2(x_R)]\\ &\quad + (1-\alpha)[J_0(x_L)+J_2(x_L)]\\ \bar{\rho}_t(r,\omega) &= \alpha[J_0(x_R)+J_2(x_R)]\\ &\quad + (1-\alpha)[J_0(x_L)-J_2(x_L)] \quad (8)\end{aligned}$$

where $x_R = \omega r/c_R(\omega)$, $x_L = \omega r/c_L(\omega)$, and subscripts v, r and t, respectively, refer to the vertical, radial and

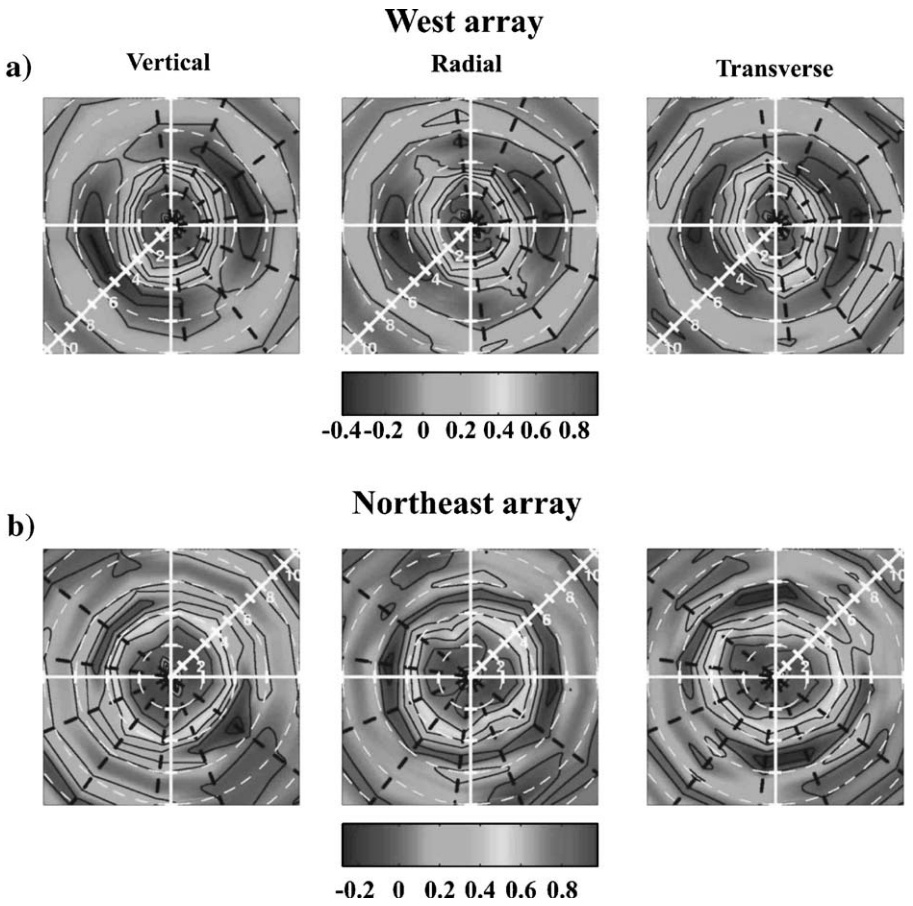

Fig. 4. Correlation coefficients represented in polar coordinates in function of the frequency ω and the azimuth φ for the three components of motion of the west (a) and northeast (b) semicircular arrays. White vertical, horizontal and oblique frequency axes are oriented N–S, E–W and SW–NE, respectively. Black dashed lines represent the azimuths of the lines connecting the couples of stations used.

transverse components of the motion. J_0 and J_2 are the zero and second-order Bessel functions, $c_R(\omega)$ and $c_L(\omega)$ are the Rayleigh and Love waves phase velocities and α is the proportion of Rayleigh wave ranging from 0 to 1.

The estimation of $c_R(\omega)$, $c_L(\omega)$ and α can be thought of as an inverse problem, the data of which are the correlation coefficients. This is a functional and slightly non-linear problem which can be solved using a generalized least squares approach (Tarantola and Valette, 1982) following Métaxian et al. (1997). We can note that the correlation coefficients of the vertical component depend only on $c_R(\omega)$, which can thus be estimated independently of the horizontal components, for which $c_R(\omega)$, $c_L(\omega)$ and α are all involved. The drawback of such a procedure is that it yields two different estimations of the Rayleigh velocities that are not always compatible (e.g. Métaxian et al., 1997).

In this study, the three components have been inverted simultaneously in order to incorporate all the information and to obtain a better trade-off between errors. The least-squares approach relies on the assumption that data and unknowns are Gaussian random elements. In the case of the unknown functions $c_R(\omega)$ and $c_L(\omega)$, the a-priori covariance is defined through a kernel $C(\omega, \omega')$ which is the covariance of the phase velocity (c_R or c_L) at frequency ω and that at ω'. $C(\omega, \omega')$ can be expressed as:

$$C(\omega,\omega') = \sigma(\omega)\sigma(\omega')f(\omega,\omega') \tag{9}$$

where $\sigma(\omega)$ is the standard deviation of $c_R(\omega)$ or $c_L(\omega)$ and $f(\omega,\omega')$ is the correlation which can be written as:

$$f(\omega,\omega') = g(x) \tag{10}$$

with:

$$x = \frac{1}{\xi}\log\frac{\omega'}{\omega} = \frac{1}{\xi}(\log\omega' - \log\omega) \tag{11}$$

where ξ is a smoothing length, and g is a real, even, continuous, and square integrable function of the

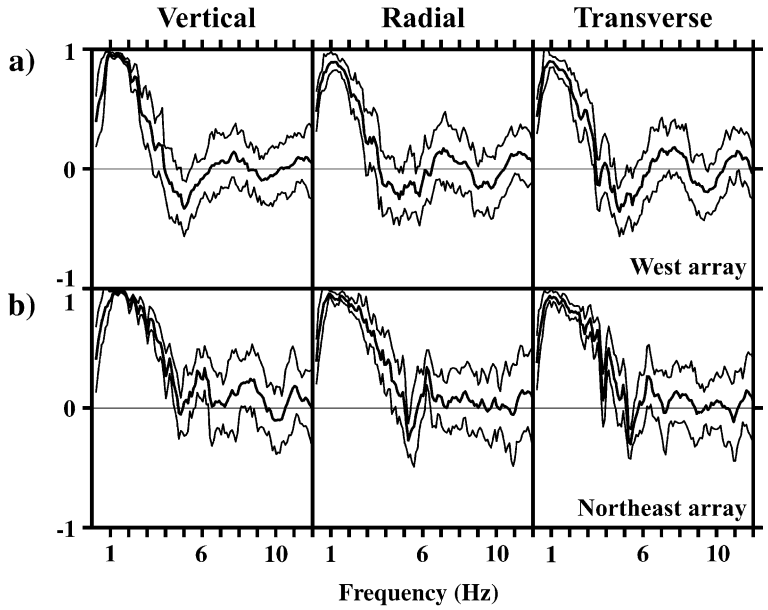

Fig. 5. Azimuthally averaged correlation coefficients $\bar{\rho}(r, \omega)$ (thick lines) and ± 1 standard deviation $\bar{\sigma}_f$ (thin lines) for the three components of motion obtained for the W (a) and NE (b) arrays.

variable x, which verifies $g(0)=1$. To ensure that C is a covariance kernel, the Fourier transform of g, which is also real and even, must be in addition positive (as a consequence of Bochner's theorem). We have used either $g(x) = \exp\left(-\frac{x^2}{2}\right)$ or $g(x) = \exp(-|x|)(\cos x + \sin|x|)$. Note that taking log ω instead of ω as variable increases the regularization at high frequencies, for which the resolution is poorer. A useful trick in implementing non-linear least-squares approach is to define new variables. For instance, the proportion of Rayleigh wave α ranges from 0 to 1, and is a priori equi-partitioned. Thus, it cannot be considered as a Gaussian variable. The point is to assign a Gaussian probability density law to the new variable y defined as $y = Erf^{-1}(2\alpha - 1)$ (so $\alpha = (1 + Erf\ y)/2$). It makes α equi-partitioned and allows the a posteriori uncertainties to be easily derived through a standard covariance analysis.

The results of the inversions are shown in Fig. 6. For the NE array, the particular shape of the correlation coefficients leads to two different solutions, A and B, of the inverse problem depending on the starting model. Solution A fits the peak near 6 Hz, whereas solution B does not. Hence, the inversion alone cannot determine the final solution and more information is needed for. As can be noticed in Fig. 6, the Rayleigh and Love phase velocities are lower at the W array. We can also note that the proportions of Rayleigh wave slightly differ between the arrays: about 54% for the NE and 49% for the W.

To estimate the velocity models from the dispersion curves, we used the programs developed by Herrmann and Ammon (2002). By trial-and-error we determined an approximate model with a minimal number of layers that reasonably adjusts the phase velocities, and then we improved it by using the inversion program. Fig. 7 and Table 1 display the obtained velocity models, which include at both sites five layers over a half-space, and the corresponding dispersion curves. In both sites, the fit between the observed and calculated Rayleigh velocities is good. In contrast, the fit for the Love dispersion curves is good only for the W array, but is poor for the NE array, especially in the case of solution A. The model for the W array is consistent with the one obtained by seismic refraction, while it is not possible to compare the models for the NE array due to the great distance between the array and the seismic refraction line.

5. Site effects analysis at Arenal and Masaya volcanoes

Three-component seismograms of harmonic tremor recorded by the W radial array and corresponding spectra are displayed in Fig. 8. While the frequencies of the peaks remain constant, there are strong variations in the waveform and in the relative amplitude of the spectral peaks at short distances. For example, in the vertical component of stations PW04 to PW09 the amplitude of the peak at 3 Hz is higher than the one

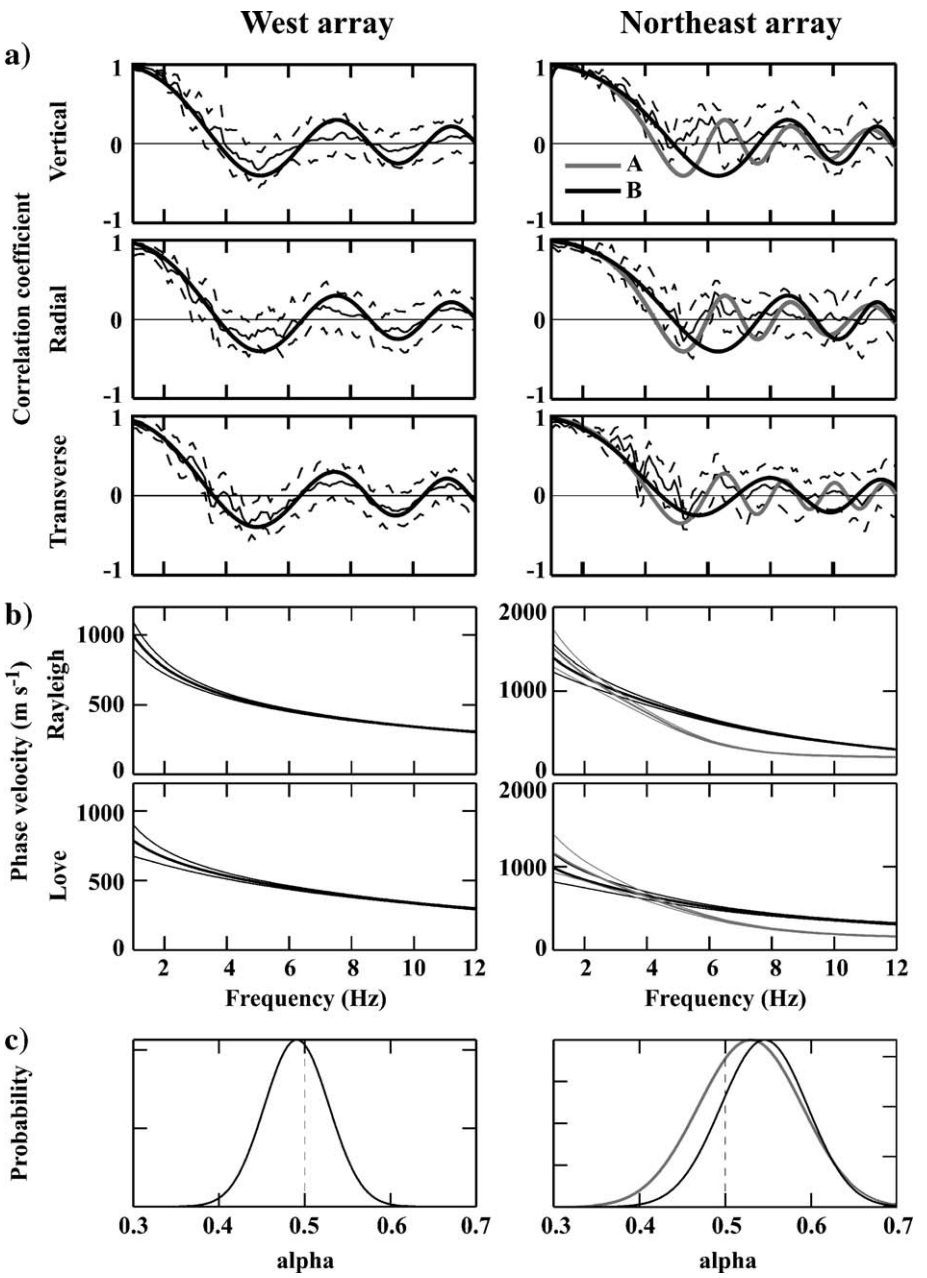

Fig. 6. (a) Fit of the theoretical correlation coefficients (thick lines) with the observed ones (thin lines) and associated errors (dash lines) for the W (left) and NE (right) arrays. (b) Estimated phase velocities (thick lines) of the Rayleigh and Love wave and corresponding errors (thin lines). (c) Probability functions associated to the proportion α of Rayleigh wave. The dash line ($\alpha = 0.5$) represents equal proportions of Rayleigh and Love waves. For the NE array, the two solutions obtained in the inverse problem, A (gray) and B (black), are shown.

at 1.5 Hz, while the amplitudes of both peaks are similar at PW02 and PW03. These local amplitude variations produce important distortions in the energy curves as a function of distance to the source, as shown in Fig. 9. The energy of the three components of movement is far from decreasing smoothly, as normally expected. Similar observations were obtained for the E radial array by Mora et al. (2001).

While the regularly spaced spectral peaks are interpreted as source effects (Benoit and McNutt, 1997; Hagerty et al., 2000; Lesage et al., 2004), the local variations in the peak amplitude are related to the geological structure (Mora et al., 2001; Mora, 2003). We analysed this site effects using the H/V spectral ratio method, which consists in calculating the ratio of the horizontal and vertical component spectra of micro-

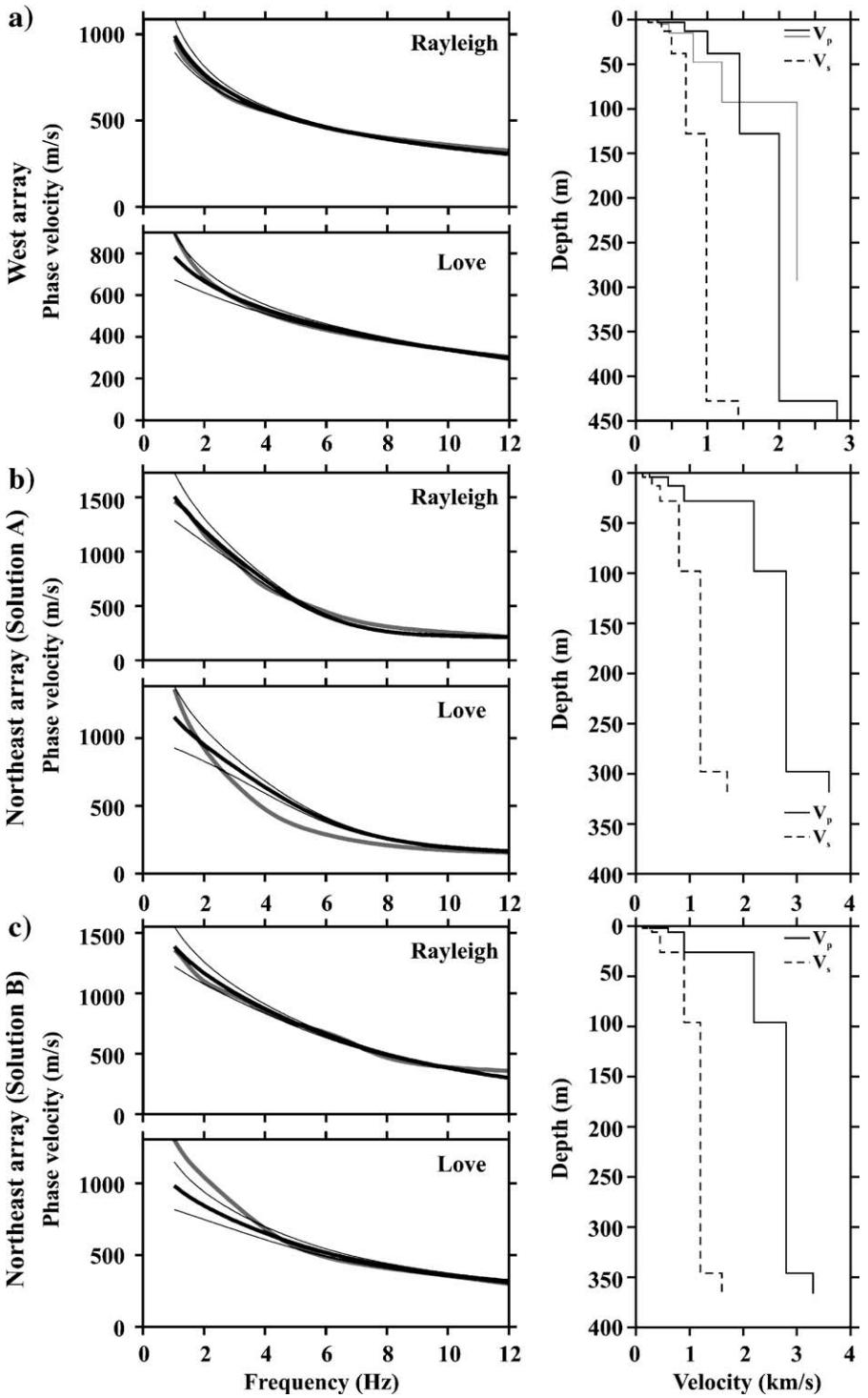

Fig. 7. Right: Velocity structure obtained by fitting the dispersion curves for the West array (a) and solutions A (b) and B (c) obtained for the NE array. The gray line represents a P-wave velocity model obtained by seismic refraction surveys. Left: Observed dispersion curves (black thick lines), and corresponding errors (thin lines), compared to the phase velocities calculated with the velocity models (gray lines).

Table 1
Structure models obtained from the inversion of Rayleigh and Love dispersion curves

Thickness (m)			V_p (km s^{-1})			V_s (km s^{-1})			Geological interpretation
W	NE A	NE B	W	NE A	NE B	W	NE A	NE B	
3	4	2	0.3	0.25	0.25	0.17	0.13	0.12	Tephra deposits composed mainly
10	9	4	0.68	0.6	0.6	0.36	0.3	0.32	of ash fall and pyroclastic flow
25	20	20	1	0.9	0.9	0.5	0.45	0.45	deposits with variable degrees
90	70	70	1.45	2.2	2.2	0.7	0.8	0.83	of consolidation
300	250	250	2	2.8	2.8	0.98	1.2	1.18	Lava flows and lava breccias
∞	∞	∞	2.81	3.6	3.3	1.43	1.7	1.6	Pre-Arenal Pliocene volcanic rocks

tremor recorded at a single station (Nakamura, 1989). Many works demonstrated that this method provides good estimates of the fundamental resonance frequency of the local structure (e.g., Lermo and Chávez-García, 1994; Theodulidis et al., 1996; Lachet et al., 1996). However the magnitude of the amplification is not reliable (Lachet and Bard, 1994). Mora et al. (2001) showed that reliable H/V ratios could be obtained from different types of seismo-volcanic events, especially those with broad spectra, such as background noise or spasmodic tremor, for which the variability of the ratios is smaller.

We selected a set of spasmodic tremor signals recorded by the W radial array and windowed in 20 s slices. The Fourier transform of each slice was calculated and smoothed by a 0.4 Hz wide moving window. The horizontal term in the H/V ratio is the geometrical average of the two horizontal component spectra. Then, assuming a lognormal distribution of spectral ratios (Field and Jacob, 1995), the logarithmic average and the corresponding standard deviation of the H/V ratios were calculated. Results show that the H/V spectral ratios from PW01 to PW08 present a marked peak at about 1.5 Hz indicating a clear site effect at this frequency (Fig. 10). In contrast, at PW09 and PW10 the H/V spectral ratios are almost constant. A moderate amplification at 13 and 10 Hz can be noted at PW11 and PW12, respectively.

In order to investigate the relationship between the observed spectral ratios and the structure, we calculated the theoretical transfer functions at each station of the W radial array. We used the reflectivity method (Kennett and Kerry, 1979) for vertically incident S-waves and took the corresponding local velocity models from the seismic refraction results. Following Nakamura (1989), the peaks in the H/V spectral ratios are generally associated with the amplification of the horizontal components of the seismic waves related to resonance effects of the shallow structure. Thus, the transfer function of vertically incident S-waves usually presents peaks at the same frequencies as those of the H/V spectral ratios. Results show a fairly good agreement between the fundamental peaks frequency of the H/V spectral ratios and the theoretical transfer functions for PW01, PW02 and PW06 (Fig. 10). For PW03, PW04 and PW05 the peak of the theoretical transfer function is shifted towards low frequencies, while for PW08 the peak is slightly shifted towards higher frequencies. At PW09 and PW10 there is no agreement between the H/V spectral ratios and the theoretical transfer functions. From PW11 to PW14 the transfer functions do not show any peak at low frequencies in agreement with the H/V spectral ratios.

We carried out a comparative analysis of the site effects at Masaya shield volcano using data from a 2.5-km-long linear array, which was deployed in 1993 on the north flank of Santiago crater (Métaxian et al., 1997). Smoothly decaying curves of the tremor energy as a function of the distance from the active crater were obtained for this array. Métaxian et al. (1997) showed that the shape of these curves can be explained by predominant surface waves from a shallow source and attenuation factors of 14 and 31 at 2 and 3 Hz, respectively. The H/V spectral ratios calculated along this array (Fig. 11) appear relatively constant with respect to frequency at the reference station and stations 2, 5, 6, and 7. Small peaks are observed at about 1.3 Hz for stations 1, 3, 4, and at 2 Hz for stations 9 and 10. The ratios obtained at Masaya have slightly lower standard deviations than those of Arenal (~1.3 vs. ~1.5). Furthermore, the H/V ratios do not display strong variations between contiguous stations and are generally smoother than the Arenal ones.

6. Discussion

We have explored part of the shallow structure at Arenal volcano and its influence on the volcanic wavefield by combining three different methods: seismic refraction surveys, inversion of surface waves disper-

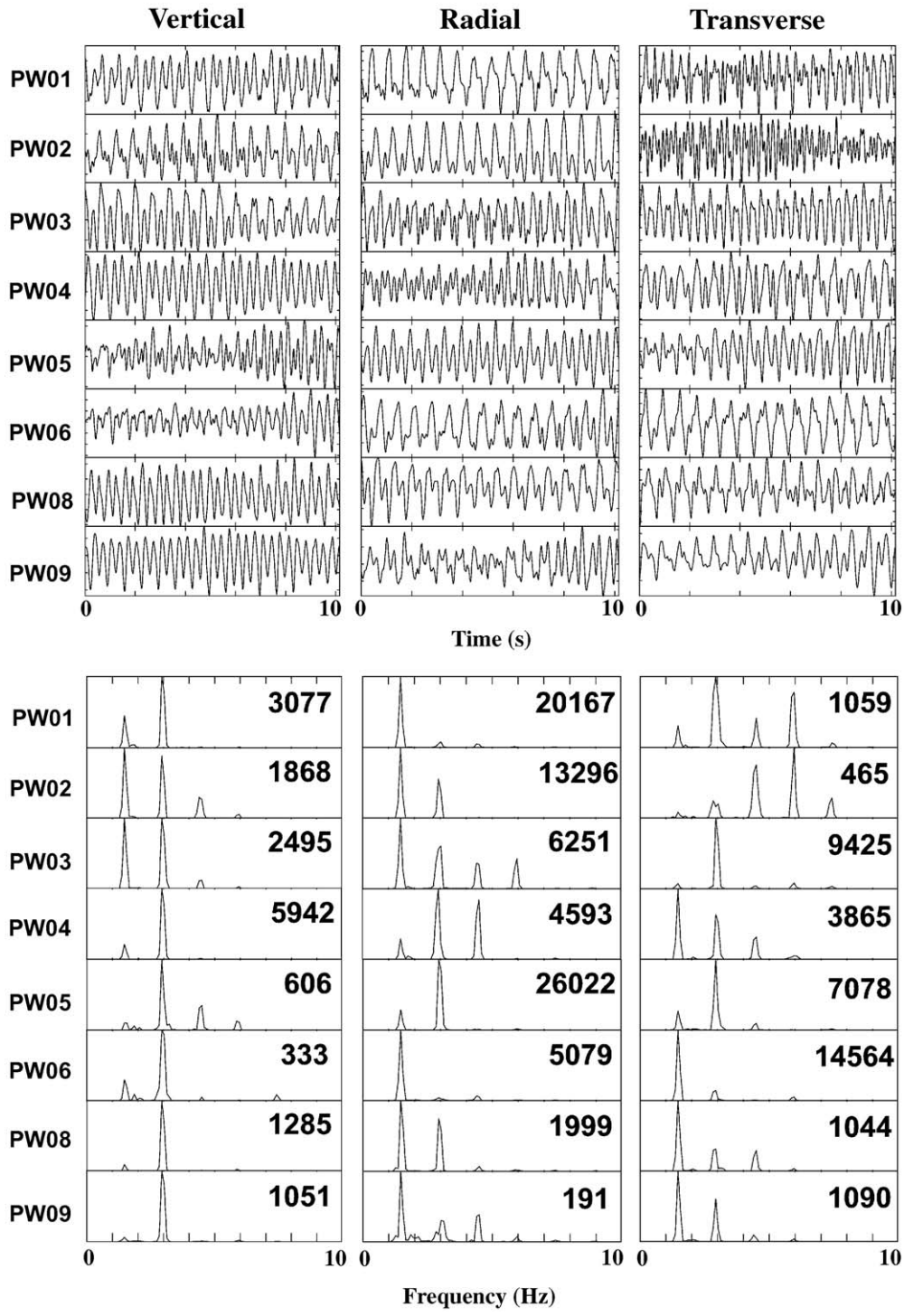

Fig. 8. Three component seismograms (top) and corresponding normalized power density spectra (bottom) of a harmonic tremor section recorded along the first part of the W radial array. The numbers at the upper right corner of the spectra indicate the maximal amplitude. No records are available at station PW07 because of a recorder failure.

sion curves and the H/V spectral ratios. Seismic refraction models show complex sequences in which layer thicknesses as well as P-wave velocities change significantly over short distances (few tens of meters). P-wave velocities are generally low (V_p<2.4 km s^{-1}), especially for the W radial array where the shallow

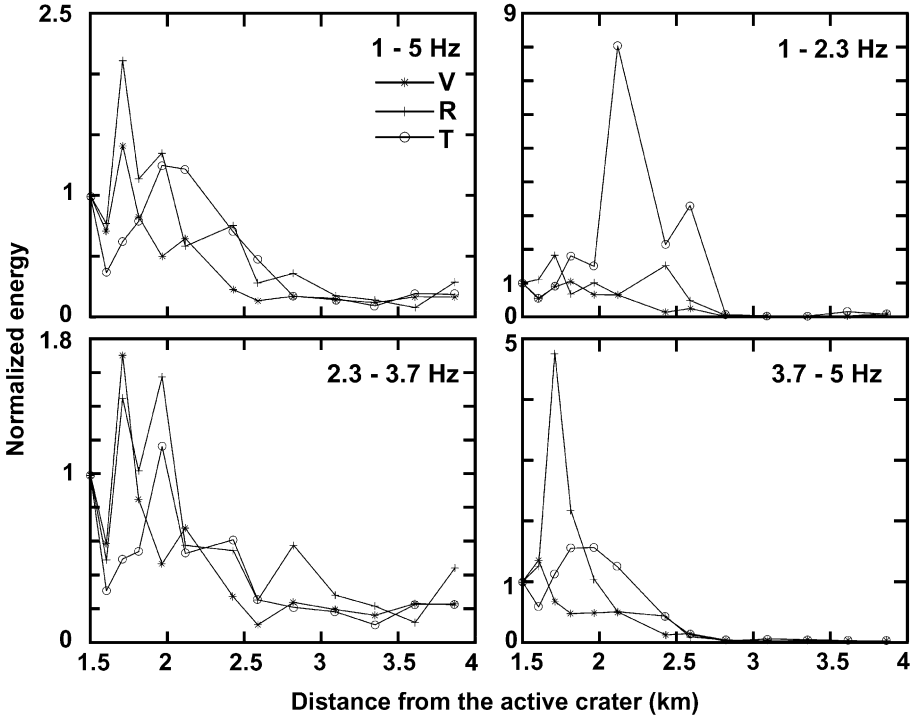

Fig. 9. Tremor energy as a function of the distance from the active crater along the W radial array in several frequency bands. All the calculated energies are normalized by the corresponding values at station PW01. V: vertical, R: radial, T: transverse component.

structure is composed of poorly consolidated epiclastic and pyroclastic deposits and breccias. This contrasts with the structure beneath the E radial array where a 50-m-thick layer with low P-wave velocity underlays in many places a layer with velocity greater than 3 km s^{-1} possibly composed of lava flow deposits.

Both the theoretical transfer functions and the H/V spectral ratios display changes along the W radial array. These features are also related to strong lateral and vertical heterogeneities of the geological structure. At many sites, the fundamental resonance frequencies, as obtained by the two methods, are consistent. The agreement is generally better where the impedance contrast is high enough to produce a strong resonance effect, and consequently a sharp peak. This is the case at stations PW02, PW06 and PW08 that show a marked peak at 1.2 Hz (Fig. 10). As the seismic refraction method requires marked velocity contrasts, the sharper are the discontinuities, the more reliable is the estimation of the layer thicknesses and velocities. On the other hand, where the impedance contrast is weak, the peaks in the H/V spectral ratios are not clear and the resolution of the seismic refraction model is poor. This situation can explain most of the disagreements between the H/V spectral ratios and the theoretical transfer functions.

Another source of discrepancy between the theoretical transfer functions and H/V spectral ratios are the 2-D and 3-D site effects. For example, on the east profile the structure abruptly changes at a distance of 600 m from the upper end, where a new layer (V_p=2.1–2.4 km s^{-1}) appears beyond a low velocity area. On the western profile a wedge-like layer (V_p=1 km s^{-1}) takes place at distances from 600 to 1000 m. A lenticular structure, which is probably associated with a paleo-valley corresponding to the ancient drainage of the Arenal paleo-river (Borgia et al., 1988), can be seen at distances between 1800 m and 2600 m. The seismic anomalies, which may correspond to fault or fracture zones, induce perturbations in the seismic refraction data, yielding less accurate models. This could explain the fact that, at stations PW03, PW04 and PW05, the fundamental resonant frequency derived by the H/V spectral ratios near 1 Hz does not agree with the one of the theoretical transfer function. The lateral heterogeneities in the structure can explain other inconsistencies, either at the ends of the seismic refraction profile or at stations PW13 and PW14, which were located about 50 m away from the refraction line.

At Masaya volcano the H/V spectral ratios are more regular than those of Arenal (Fig. 11). Most of them are

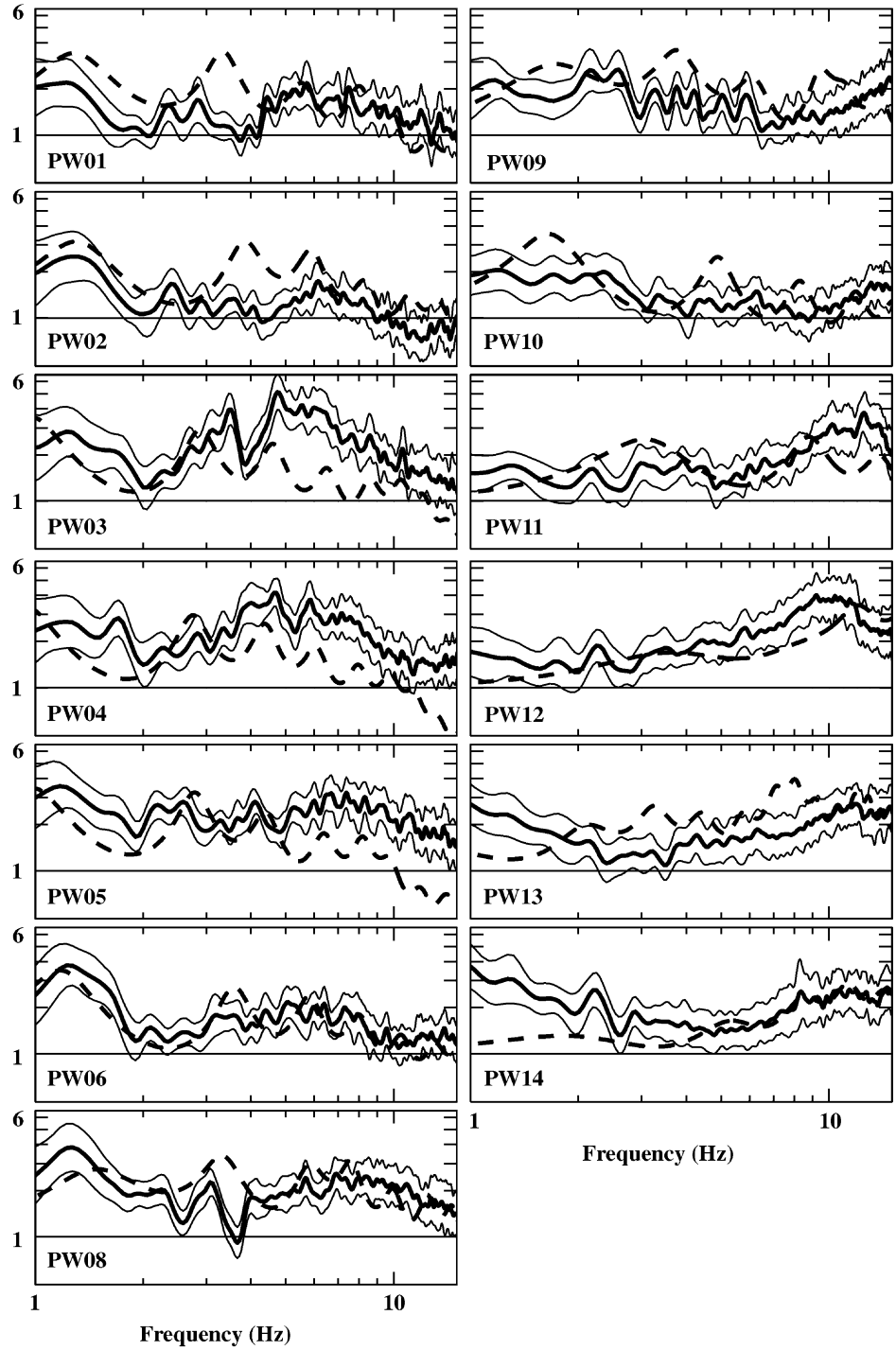

Fig. 10. Mean H/V ratios (solid lines), calculated with 43 20.48 s long slices of spasmodic tremor, mean ratios ± 1 standard deviation (thin lines), and theoretical S-wave transfer functions (dashed lines) for the stations of the West radial array.

almost constant, especially at low frequency, like the reference station or station 6, or present a wide bulge, like stations 2, 3 and 8. This suggests a more homogeneous structure with low impedance contrasts, which is consistent with the smooth and regular decrease of the tremor energy with respect to the distance to the source. Some peaks are observed mainly at stations 1, 4, 9 and 10. They may be related either to topographic effects, as

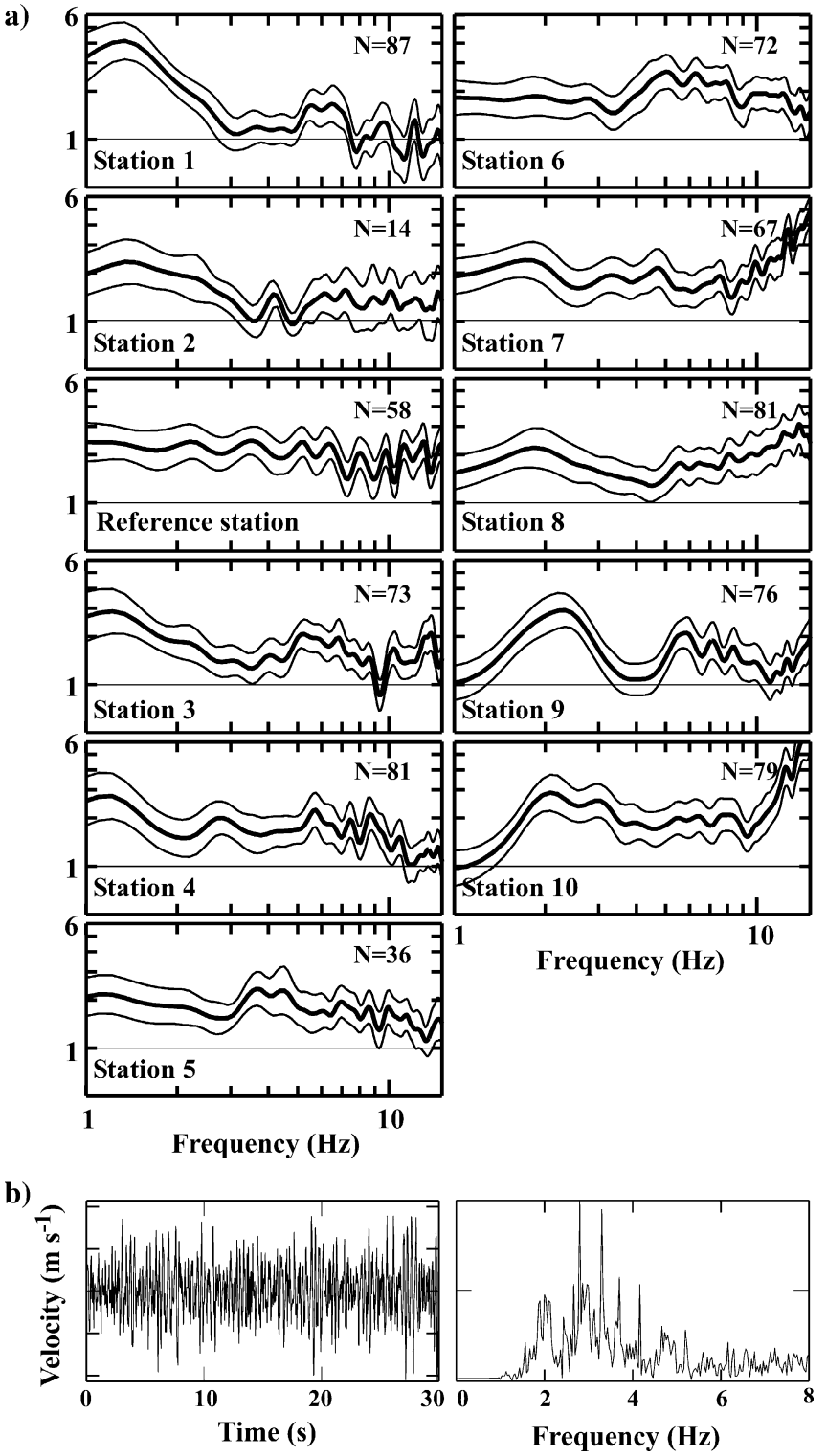

Fig. 11. (a) Same as Fig. 10 for the radial array deployed at Masaya volcano (Nicaragua). *N* represents the number of tremor slices used. (b) Tremor used for the H/V estimates have most of the energy concentrated between 1 and 5 Hz, as shown in the spectrum of one of the slices.

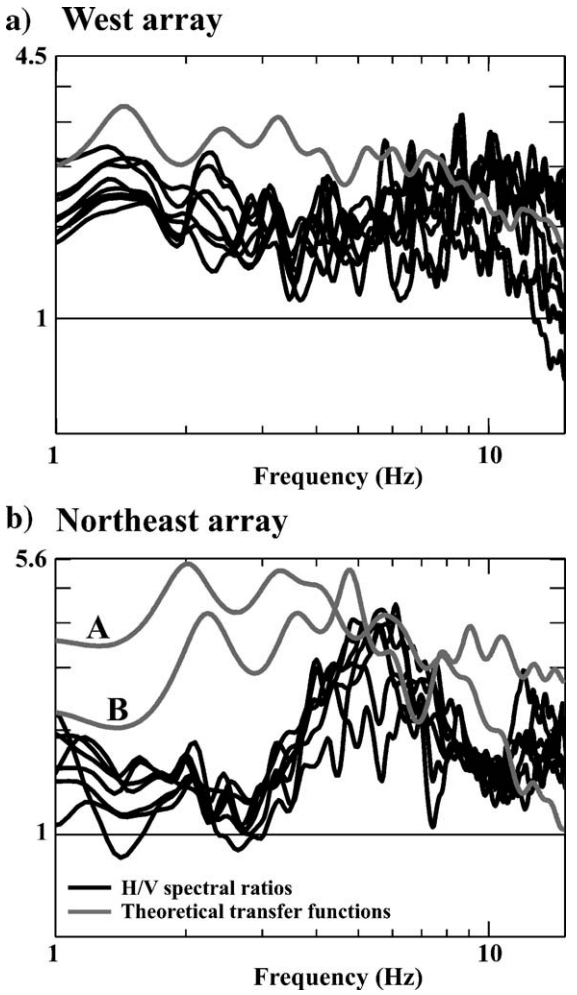

Fig. 12. H/V spectral ratios (black lines), calculated for all the stations of the W (a) and NE (b) semicircular arrays, and theoretical S-wave transfer functions (gray lines). For the NE array, the transfer functions obtained from velocity model solutions A and B are shown.

for station 1, or to local increases of the impedance contrasts due to deposits of other materials, or even to weathering of the shallow lava layers.

The differences in the spectral ratios behaviour between Arenal and Masaya volcanoes are clearly related to the involved geological structures. At Arenal volcano the arrays were located at the lower part of the flanks, where the geological structure mainly consists of a heterogeneous and unconsolidated tephra apron presenting strong lateral and vertical variations, which produces significant seismic site effects. In contrast, the linear array at Masaya was deployed in proximity to the Santiago active crater where the Masaya volcanic edifice is composed predominantly by a thick tholeiitic lava sequence that does not produce strong seismic site effects.

The third method we have used is the spatial correlation method (Aki, 1957). We have estimated the phase velocities of the Rayleigh and Love waves at two sites of the west and northeast flanks of Arenal volcano, from which we have derived shallow 1-D velocity models. To test the consistency of the results, we have calculated the theoretical S-wave transfer functions from the velocity models and have compared them with the H/V spectral ratios computed for all stations of the semicircular arrays (Fig. 12). While some details of the H/V ratios change from one site to another, the overall shape of the ratios remains similar over all the stations of each array. This suggests that there are no major lateral heterogeneities in the underlying structures. At the W array, the H/V ratios show a peak at about 1.5 Hz that agrees with the one of the theoretical transfer function, which demonstrates that the model is consistent with the observed site effect.

For the NE array, from which we have obtained two solutions for the velocity models, the H/V spectral ratios show a maximum between 5 and 6 Hz. The transfer function calculated with model A has only a small secondary peak in this frequency interval. In contrast, the model B transfer function displays at 4.8 Hz a sharp peak that is more consistent with the H/V spectral ratios. This observation leads us to prefer model B among the two solutions obtained by inversion of the phase velocities. The difference between the two solutions can be related to the existence of a marked increase of the correlation coefficients at about 6 Hz for the three components. While the coefficients calculated from model A roughly fit this peak, the model B coefficients do not adjust it at all. A similar peak in the correlation coefficients at about 5 Hz was observed at Kilauea volcano and was interpreted as the effect of narrow-band body waves superimposed to the surface wavefield (Saccorotti et al., 2003). At Arenal, the detection of a site effect by the spectral ratio method suggests that the resonance of the shallow structure can produce an increase in the correlation due to in-phase oscillations of the whole surface over the area. This alternative interpretation, which does not take account of the 6 Hz peak in the correlation coefficients, supports the choice of model B.

7. Conclusions

By carrying out a combination of three methods, different features of the Arenal structure have been obtained and their strong influence on the seismic wavefield have been demonstrated. The seismic refrac-

tion survey produces the more detailed images of the structure. Nevertheless, its penetration depth is limited by the power of the source used and the length of the experimental survey. Furthermore, scattering effects may yield strong attenuation of the body waves amplitudes and prevent precise time arrival picking (Wegler and Lühr, 2001). The SPAC method is relatively easy to carry out and gives robust estimations of the P and S waves velocities models within the first hundreds meters, although its vertical resolution is poor. The H/V spectral ratios method is easy to implement whenever three-components records are available and its use is crucial to detect marked site effects. Nevertheless, only the significance of the fundamental resonance peak has been well established.

Vertical and lateral heterogeneities at a scale of a few tens or hundreds of meters have been revealed by detailed seismic refraction surveys and H/V spectral ratios. Both methods strongly depend on the impedance contrast between layers and they are consistent when the contrast is high enough. Where the impedance contrast is low, the resolving power of seismic refraction is poor and the H/V spectral ratios exhibit no marked peaks. Complex shape of the H/V ratios can also be explained by 2-D or 3-D structural heterogeneities, which have not been considered in this study. These heterogeneities may be related to faults, paleovalleys or lenticular structures.

Whatever the origin of the site effects, they disturb many features of the seismic waves at the surface, such as their amplitude, polarization, incidence angle or apparent slowness vector, which may lead to misinterpretations. While these effects are moderate in relatively homogeneous structures, such as that of Masaya volcano, they can produce strong perturbations in case of a structure like that of Arenal, up to the point of making some observations unusable.

The application of the spatial correlation method combined with the H/V spectral ratios leads us to question the common assumptions that surface waves propagate in plane layers and that the fundamental modes of Rayleigh and Love waves are dominant in the wavefield. We have observed that the resonance of shallow layers induce an increase of the correlation coefficients near the resonance frequency, which leads to spurious velocity models. The H/V spectral ratio method can help detecting strong lateral heterogeneities underneath the semicircular arrays and testing the plane layers hypothesis. Furthermore the comparison of the ratios with the theoretical transfer function calculated with the estimated structure can be useful to support or reject the obtained velocity models.

Acknowledgments

We thank the staff of the Instituto Costarricense de Electricidad (ICE) and the Observatorio Sismológico y Vulcanológico de Arenal y Miravalles (OSIVAM) for their logistical support during the field work and for the seismic refraction and electric surveys they carried out. We also acknowledge the Area de Conservación Arenal staff for the facilities provided during the fieldwork. Special thanks to Pierre-Yves Bard for his support and guide for the site effects analysis. Comments of the two anonymous reviewers help to improve substantially the manuscript. We also thanks the comments and review carried out by Benjamin Van Wyk de Vries and Gerardo Soto Bonilla which help us to improve the manuscript. This study was supported by the Programme Régional pour la Prévention du Risque Volcanique en Amérique Centrale (PREVO-MAE), the Programme National de Recherche sur la Prévision et la Prévention des Risques Naturels (PNRN-INSU), the Centre de Recherches Volcanologiques (CRV-CNRS), the Université de Savoie, the Institut de Recherche pour le Développement (IRD) and the Universidad de Costa Rica (UCR).

References

Aki, K., 1957. Space and time spectra of stationary stochastic waves, with special reference to microtremors. Bull. Earthq. Res. Inst. Univ. Tokyo 25, 415–457.

Alvarado, G.E., Barquero, R., 1987. Las señales sísmicas del Volcán Arenal (Costa Rica) y su relación con las fases eruptivas (1968–1986). Cienc. Tecnol. 11, 15–35.

Alvarado, G.E., Soto, G.J., 2002. Pyroclastic flow generated by crater-wall collapse and outpouring of the lava pool of Arenal Volcano. Costa Rica Bull. Volcanol. 63, 557–568.

Alvarado, G.E., Carboni, S., Cordero, M., Avilés, E., Valverde, M., Leandro, C., 2003. Estabilidad del cono y comportamiento de la fundación del edificio volcánico del Arenal (Costa Rica). Bol. Observ. Sismol. Vulcanol. Arenal Miravalles 14 (26), 21–73.

Benoit, J.P., McNutt, S.R., 1997. New constraints on source processes of volcanic tremor at Arenal Volcano, using broadband seismic data. Geophys. Res. Lett. 24, 449–452.

Bettig, B., Bard, P.-Y., Scherbaum, F., Riepl, J., Cotton, F., Cornou, C., Hatzfeld, D., 2003. Analysis of dense array noise measurements using the modified spatial auto-correlation method (SPAC). Application to the Grenoble area. Boletin de Geofisica Teorica e Applicata 42, 281–304.

Borgia, A., Poore, C., Carr, M.J., Melson, W.G., Alvarado, G.E., 1988. Structural, stratigraphic and petrologic aspects of the Arenal-Chato volcanic system, Costa Rica: evolution of a young stratovolcanic complex. Bull. Volcanol. 50, 86–105.

Chouet, B., 1996. Long-period volcano seismicity: its source and use in eruption forecasting. Nature 380, 309–316.

Chouet, B., De Luca, G., Milana, G., Dawson, P., Martini, M., Scarpa, R., 1998a. Shallow velocity structure of Stromboli volcano, Italy, derived from small-aperture array measurements of Strombolian tremor. Bull. Seismol. Soc. Am. 88, 653–666.

Chouet, B., Dawson, P., De Luca, G., Martini, M., Milana, G., Saccorotti, G., Scarpa, R., 1998b. Array analyses of seismic wavefields radiated by eruptive activity at Stromboli volcano, Italy. CNR-Gruppo Nazionale per la Vulcanologia. Felici Editore, Piza, Italy.

Del Pezzo, E., Guerra, I., Lo Bascio, A., Luongo, G., Nappi, G., Scarpa, R., 1974. Microtremors and volcanic explosions at Stromboli—Part 2. Bull. Volcanol. 38, 1023–1036.

Falsaperla, S., Martinelli, B., Schick, R., 1992. Seismic activity at Stromboli (Southern Italy) for the period 1983–1986. In: Gasparini, P., Scarpa, R., Aki, K. (Eds.), Volcanic Seismology. Springer-Verlag, Berlin.

Ferrazzini, V., Aki, K., Chouet, B., 1991. Characteristics of seismic waves composing Hawaiian volcanic tremor and gas piston events observed by near-source array. J. Geophys. Res. 96, 6199–6209.

Field, J.E., Jacob, H., 1995. A comparison and test of various site-response estimation techniques, including three that are not reference-site dependent. Bull. Seismol. Soc. Am. 85, 1127–1143.

Goldstein, P., Chouet, B., 1994. Array measurements and modeling of sources of shallow volcanic tremor at Kilauea Volcano, Hawaii. J. Geophys. Res. 99, 2637–2652.

Gordeev, E.I., Melnikov, Y.Y., Sinitsy, V.I., Chebrov, V.N., 1989. Volcanic tremor of Kliuchevskoi volcano (1984 Eruption). In: Latter, J.H. (Ed.), Volcanic Hazards, Assessment and Monitoring. Springer-Verlag, Berlin.

Gordeev, E., Saltykov, V.A., Sinitsyn, V.I., Chebrov, V., 1990. Temporal and spatial characteristics of volcanic tremor wavefields. J. Volcanol. Geotherm. Res. 40, 89–101.

Gordeev, E., 1993. Modeling of volcanic tremor as explosive point sources in a single-layered, elastic half-space. J. Geophys. Res. 98, 19687–19703.

Hagerty, M.T., Schwartz, S.Y., Garcés, M.A., Protti, M., 2000. Analysis of seismic and acoustic observations at Arenal Volcano, Costa Rica, 1995–1997. J. Volcanol. Geotherm. Res. 101, 27–65.

Hagiwara, T., Omote, S., 1939. Land creep at Mt. Tyausu-Yama (Determination of slip plane by seismic prospecting). Bull. Earthq. Res. Inst. 17, 118–137.

Hellweg, M., 2003. The polarization of volcanic seismic signals: medium or source? J. Volcanol. Geotherm. Res. 128, 159–176.

Herrmann, R.B., Ammon, Ch., 2002. Computer programs in Seismology: Surface waves, receiver functions and crustal structure (Version 3.15). St. Louis Univ., St. Louis, Mo.

Kedar, S., Kanamori, H., Sturtevant, B., 1998. Bubble collapse as the source of tremor at Old Faithful Geyser. J. Geophys. Res. 103, 24283–24299.

Kennett, B.L.N., Kerry, N.J., 1979. Seismic waves in a stratified half-space. Geophys. J. R. Astron. Soc. 57, 557–583.

La Rocca, M., Del Pezzo, E., Simini, M., Scarpa, R., De Luca, G., 2001. Array analysis of seismograms from explosive sources: evidence for surface waves scattered at the main topographical features. Bull. Seismol. Soc. Am. 91, 219–231.

Lachet, C., Bard, P.-Y., 1994. Numerical and theoretical investigations on the possibilities and limitations of Nakamura's technique. J. Phys. Earth 42, 377–397.

Lachet, C., Hatzfeld, D., Bard, P.-Y., Theodulidis, N., Papaioannou, C., Savvaidis, A., 1996. Site effects and microzonation in the city of Thessaloniki (Greece) comparison of different approaches. Bull. Seismol. Soc. Am. 86, 1692–1703.

Leandro, C., Alvarado, G.E., 1999. Estudio Geológico-Geofísico de una sección oriental y occidental en el volcán Arenal. Bol. Observ. Sismol. Vulcanol. Arenal Miravalles. 20–21, 48–58.

Lermo, J., Chávez-García, J.F., 1994. Are microtremors useful in site response evaluation? Bull. Seismol. Soc. Am. 84, 1350–1364.

Lesage, Ph., Mora, M., Alvarado, G., Métaxian, J.-Ph., 2004. Complex behaviour and evidence of double source for the volcanic tremor at Arenal volcano. Costa Rica, EGU, Nice.

Melson, W.G., Sáenz, R., 1968. The eruption of Volcán Arenal, Costa Rica: Preliminary summary of field and laboratory studies. Smithsonian Institution Center for Short-Lived Phenomena, Report 7. Open file report, Departamento de Geología. Instituto Costarricense de Electricidad, San José.

Métaxian, J.-P., Lesage, P., Dorel, J., 1997. Permanent tremor of Masaya volcano, Nicaragua: wavefield analysis and source location. J. Geophys. Res. 102, 22529–22545.

Métaxian, J.-Ph., Lesage, Ph., Valette, B., 2002. Locating sources of volcanic tremor and emergent events by seismic triangulation: application to Arenal volcano, Costa Rica. J. Geophys. Res. 107, 2243.

Mora, M., 2003. Etude de la structure superficielle et de l'activité sismique du volcan Arenal, Costa Rica. PhD Thesis, Laboratoire de Géophysique Interne et Tectonophysique, Université de Savoie. Le Bourget du Lac. 153 pp.

Mora, M., Lesage, Ph., Dorel, J., Bard, P.-Y., Métaxian, J.-Ph., Alvarado, G.E., Leandro, C., 2001. Detection of seismic site effects by using H/V spectral ratios at Arenal volcano (Cost Rica). Geophys. Res. Lett. 28, 2991–2994.

Nakamura, Y., 1989. A method of dynamic characteristics estimation of subsurface using microtremor on the ground surface. Q. Rep. RTRI 30, 25–33.

Neuberg, J., Pointer, T., 2000. Effects of volcano topography on seismic broad-band waveforms. Geophys. J. Int. 143, 243–248.

Ntepe, N., Dorel, J., 1990. Observations of seismic volcanic signals at Stromboli volcano (Italy). J. Volcanol. Geotherm. Res. 43, 235–251.

Saccorotti, G., Del Pezzo, E., 2000. A probabilistic approach to the inversion of data from a seismic array and its application to volcanic signals. Geophys. J. Int. 143, 249–261.

Saccorotti, G., Almendros, J., Carmona, E., Ibáñez, J.M., Del Pezzo, E., 2001a. Slowness anomalies from two dense seismic arrays at Deception Island volcano, Antartica. Bull. Seismol. Soc. Am. 91, 561–571.

Saccorotti, G., Maresca, R., Del Pezzo, E., 2001b. Array analyses of seismic noise at Mt. Vesuvius Volcano, Italy. J. Volcanol. Geotherm. Res. 110, 79–100.

Saccorotti, G., Chouet, B., Dawson, P.B., 2003. Shallow velocity models at Kilauea Volcano, Hawaii, determined from array analyses of tremor wavefield. Geophys. J. Intl. 152, 633–648.

Soto, G.J., Alvarado, G.E., Ghigliotti, M., 1998. El registro eruptivo de Arenal en el lapso 3000–7000 años antes del presente y nuevas deducciones sobre la edad del volcán. Bol. Observ. Sismol. Vulcanol. Arenal Miravalles 9 (17–18), 19–49.

Soto, G.J., López, D.L., Fernández, J.F., Alvarado, G.E., 1999. Caracterización geoquímica de las aguas termales del volcán Arenal (Costa Rica). Bol. Observ. Sismol. Vulcanol. Arenal Miravalles 11 (21–22), 1–20.

Soto, G.J., Alvarado, G.E., Bonilla, J., Madrigal, J., Mata, A., Ramírez, R., Rojas, L., Salazar, J., Tristán, E., Villegas, A., 2000. Las facies proximales de la gran erupción piroclástica basáltica ET-3 del volcán Arenal. Bol. Observ. Sismol. Vulcanol. Arenal Miravalles 12 (23–24/), 54–63.

Tarantola, A., Valette, B., 1982. Generalized nonlinear inverse problems solved using the least squares criterion. Rev. Geophys. Space Phys. 28, 219–232.

Theodulidis, P., Bard, P.-Y., Archuleta, R., Bouchon, M., 1996. Horizontal-to-vertical spectral ratio and geological conditions: the case of Garner Valley downhole array in Southern California. Bull. Seismol. Soc. Am. 86, 306–319.

Tsuruga, K., Yomogida, K., Honda, S., Ito, H., Ohminato, T., Kawakatsu, H., 1997. Spatial and temporal variations of volcanic earthquakes at Sakurajima volcano, Japan. J. Volcanol. Geotherm. Res. 75, 337–358.

Vandecar, J.C., Crosson, R.S., 1990. Determination of teleseismic relative phase arrival times using multi-channel cross-correlation and least-squares. Bull. Seismol. Soc. Am. 80, 150–169.

Wada, T., Ono, H., 1965. Spectral study of volcanic micro-tremors (1) Propagation of the microtremors of the first kind observed at Aso. Spec. Contrib. Geophys. Inst. Kyoto Univ. 5, 169–178.

Wegler, U., Lühr, B.G., 2001. Scattering behaviour at Merapi volcano (Java) revealed from an active experiment. Geophys. J. Int. 145, 579–592.

Weiland, A.M., Steck, L.K., Dawson, P.B., Korneev, V.A., 1995. Non-linear teleseismic tomography at Long Valley caldera, using three-dimensional minimum travel time ray tracing. J. Geophys. Res. 100, 20379–20390.